International Journal of Minerals, Metallurgy and Materials
Volume 29, Number 5, May 2022, Page 1073
https://doi.org/10.1007/s12613-022-2449-9

Invited Review

Hydrogen as a carrier of renewable energies toward carbon neutrality: State-of-the-art and challenging issues

Xuan Liu[1,2),*,✉], *Gaoyang Liu*[2),*], *Jilai Xue*[2)], *Xindong Wang*[2)], *and Qingfeng Li*[1),✉]

1) Department of Energy Conversion and Storage, Technical University of Denmark, Fysikvej 310, 2800 Kgs. Lyngby, Denmark
2) School of Metallurgical and Ecological Engineering, University of Science and Technology Beijing, Beijing 100083, China
(Received: 20 January 2022; revised: 22 February 2022; accepted: 28 February 2022)

Abstract: Energy storage and conversion via a hydrogen chain is a recognized vision of future energy systems based on renewables and, therefore, a key to bridging the technological gap toward a net-zero CO_2 emission society. This paper reviews the hydrogen technological chain in the framework of renewables, including water electrolysis, hydrogen storage, and fuel cell technologies. Water electrolysis is an energy conversion technology that can be scalable in megawatts and operational in a dynamic mode to match the intermittent generation of renewable power. Material concerns include a robust diaphragm for alkaline cells, catalysts and construction materials for proton exchange membrane (PEM) cells, and validation of the long-term durability for solid oxide cells. Hydrogen storage via compressed gas up to 70 MPa is optional for automobile applications. Fuel cells favor hydrogen fuel because of its superfast electrode kinetics. PEM fuel cells and solid oxide fuel cells are dominating technologies for automobile and stationary applications, respectively. Both technologies are at the threshold of their commercial markets with verified technical readiness and environmental merits; however, they still face restraints such as unavailable hydrogen fueling infrastructure, long-term durability, and costs to compete with the analog power technologies already on the market.

Keywords: carbon neutrality; hydrogen energy; water electrolysis; hydrogen storage; fuel cells

1. Introduction

Global energy consumption is the basis of modern civilization. Fossil fuels are the prevailing energy source that is usually converted into heat, mechanical energy, and electricity via combustion, thermal engines, and generators, respectively. Thermal engines are limited in energy conversion efficiency, which is typically less than 40% for modern power plants and 10%–20% for small engines. Another critical issue is the power production from fossil fuels generating greenhouse gas emissions. On a global scale, approximately 50 billion metric tons of greenhouse gases are emitted every year, 78% of which is from the industrial combustion of fossil fuels. These numbers have already doubled since 1970, and the increasing rate in recent years is over one billion metric tons per year [1]. Today the atmospheric concentration of CO_2 has reached 400 ppm, and the concentration of all greenhouse gases is greater than 430 ppm. Without any action, the world is projected toward 450 ppm greenhouse gases in 2030, increasing to as much as 1300 ppm by 2100.

The emission of greenhouse gases has already caused average global warming of 1.1°C since the beginning of the industrial revolution, and the warming is estimated to exceed 1.5°C over the next two decades. This will result in severe climate consequences, including heat extremes, drought, and flooding. Worldwide efforts are being made to mitigate the climate issue aiming at restraining global warming to less than 2°C, which is estimated to correspond to an extra 800 to 1000 billion metric tons of greenhouse gases or a 450 ppm limit of the greenhouse gas concentration [1].

Technologically, the immediate solution is CO_2 capture and storage (CCS). The critical challenge to deploying current CCS technologies is affordability, which is 50–120 $\$\cdot t^{-1}$ CO_2 compared with the target cost of 15–20 $\$\cdot t^{-1}$ CO_2, depending on existing technologies in different countries and industry sectors [2]. The ultimate solution is to replace fossil fuels with renewable energies, e.g., solar, wind, hydro, or biomass, which are still immature technologies facing key challenges associated with efficient energy storage at various time and power scales. Water electrolysis is regarded as a practical method of energy storage of renewable energy sources. The hydrogen, as an energy carrier, could be stored in a power scale, matching the grid with high flexibility.

Hydrogen and its combination with electrochemical energy conversion technology, the fuel cell, has been recognized as a reliable, secure, and clean technology for future energy systems. For mobile applications, hydrogen can be further stored physically; for example, as compressed gas, liquid, or metal hydrides, or alternatively, via synthesis of liquid biofuels.

*These authors contributed equally to this work.

✉ Corresponding authors: Xuan Liu E-mail: xuanliu@ustb.edu.cn; Qingfeng Li E-mail: qfli@dtu.dk

Fig. 1 schematically shows the hydrogen chain in association with renewable energy sources. Water is the medium when pure hydrogen is used, while carbon dioxide cycling is involved if other hydrogen-containing carriers, e.g., hydrocarbons and alcohols, are used. The key linking technologies of the hydrogen chain are water electrolysis, hydrogen storage, and fuel cells. The present paper is devoted to a brief review of these technologies where the emphasis is placed on state-of-the-art materials, performance, and challenges.

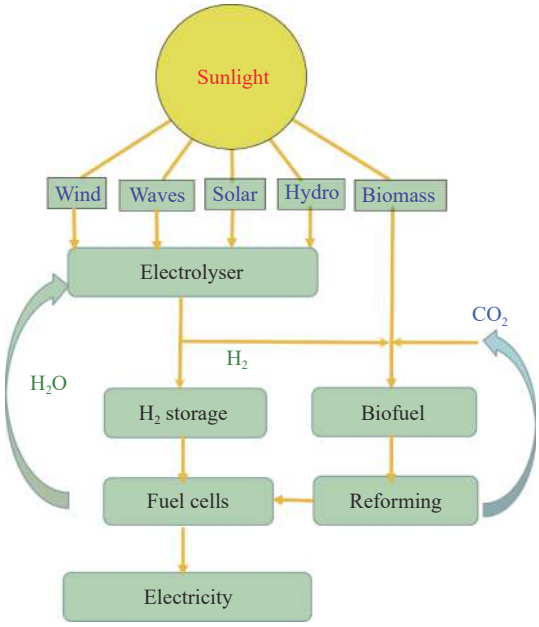

Fig. 1. Hydrogen chain in association with renewable energies where the key technologies are electrolyzer, hydrogen storage, and fuel cells.

2. Hydrogen production by electrolysis

Hydrogen production by water electrolysis was the first discovery of the electrochemical process after the invention of the voltaic pile (batteries) in 1800 [3]. From an energy storage point of view, this method is clean, scalable, and easy to operate under a dynamic mood, which are essential to matching the intermittent renewable power grid. The purity of the hydrogen obtained is also high, and water as the medium is abundant and inexpensive [4–5].

Three kinds of electrolysis cells have been invented, i.e., low-temperature alkaline electrolysis cells (AECs) [6], proton exchange membrane electrolysis cells (PEMECs) [7], and high-temperature solid oxide electrolysis cells (SOECs) [5]. The scale of AECs can be megawatts with a well-demonstrated lifetime; however, the AECs require a constant power supply. PEMECs have good dynamic performance (quick startup/shutdown and variable loads) to fit the intermittent nature of renewable sources. In general, the performance of both alkaline and proton exchange membrane (PEM) electrolyzers is greatly limited by sluggish electrode kinetics because of operation in the low-temperature range. Alternatively, high-temperature SOECs are kinetically favored and operate more efficiently, though the technology has not yet reached large-scale commercialization.

2.1. Alkaline electrolysis cells

2.1.1. Cell construction and key materials

AECs have been used to industrially produce hydrogen for over a century, and they account for the largest capacity of the installed water electrolysis worldwide. Commercial AECs have a power size up to megawatts, corresponding to a hydrogen production rate from several hundred $Nm^3 \cdot h^{-1}$ up to a thousand $Nm^3 \cdot h^{-1}$ [8].

With an alkaline electrolyte, the hydrogen evolution reaction (HER) and oxygen evolution reaction (OER) are described as follows (E^0 is the standard reaction potential) [4,7,9]:

$$\text{Cathodic HER: } 2H_2O + 2e^- \rightarrow 2OH^- + H_2,\ E^0 = -0.828\ \text{V} \quad (1)$$

$$\text{Anodic OER: } 2OH^- \rightarrow \frac{1}{2}O_2 + H_2O + 2e^-,\ E^0 = -0.401\ \text{V} \quad (2)$$

$$\text{Overall cell reaction: } H_2O \rightarrow H_2 + \frac{1}{2}O_2,\ E^0 = -1.229\ \text{V} \quad (3)$$

The electrolyte is typically 25wt%–30wt% potassium hydroxide (KOH) aqueous solutions, taking advantage of the high ionic conductivity. As shown in Fig. 2, the electrodes are immersed in the electrolyte that circulates within the cell and carries the produced gas out. During the electrolysis, the electrolyte is not consumed while water is continuously supplied. Hydrogen produced in AECs contains fine droplets of electrolyte and water vapor; drying is necessary to further purify the hydrogen.

Cathodes and anodes are most commonly made of Ni-based materials, which have reasonably low prices, high catalytic activity, and stability in alkaline electrolytes. The electrodes are in hollow structures through which the liquid electrolyte flows and circulates. The Ni-based cathode is often modified to metal alloys such as Ni–Mo and Ni–Cr–Fe. Alternative cathode catalyst materials that are in development include phosphides, sulfides, selenides, and carbides [10]. The OER requires an overpotential or high activation energy to resolve the low kinetics, which limits the efficiency of the technology [11]. The anode is also made of Ni, often coated with metal oxides.

A diaphragm between electrodes is used to separate the two product gases. This is the most critical cell component to optimize the dynamic performance when the electrolyzer cell is used in association with the fluctuating power of renewable sources. The minimum fraction of load of AECs is refrained by the diaphragm performance, which does not fully avoid the crossover of the produced gases. More cross-mixing of hydrogen and oxygen occurs under low current density operation, which reduces the energy efficiency and creates safety issues.

Conventionally, the diaphragm comprises asbestos with several millimeters thick. This material is carcinogenic and currently forbidden in more than 60 countries. Microporous

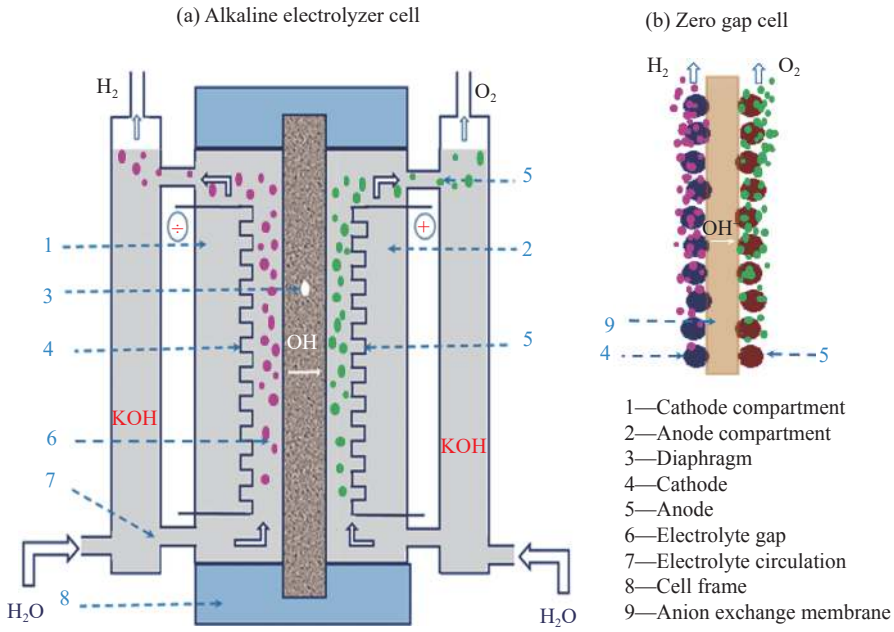

Fig. 2. (a) Schematic of alkaline electrolyzer cell constructions and (b) zero-gap cell with anion exchange membranes.

polymer substrates such as polyphenylene sulfide, usually filled by glass fibers, are alternatives. The commercial Zirfon® diaphragm is typically a polysulfone matrix containing up to 85% ZrO_2 nanopowder with a thickness of ~500 μm. This material has a porosity of approximately 60% with submicron pores, an area-specific resistance down to 0.1 Ω·cm^2 (80°C), and allows for a bubble pressure up to 0.4 MPa when filled by KOH electrolyte.

2.1.2. Performance and challenges

Current alkaline water electrolyzers typically operate with a cell voltage of 1.8–2.2 V, a current density of 0.1–0.3 A·cm^{-2}, and a working temperature of 60–80°C. This relatively low current density of operation limits the hydrogen production rate, making the system volume and weight bulky [5].

The current required to operate alkaline electrolyzers relies on the hydrogen generation rate or the scale of the electrolyzers. The energy consumption is approximately 4.5 kWh per Nm^3 H_2 (50 kWh per kg H_2) when the nominal hydrogen generation rate is greater than 10 Nm^3 H_2 per hour. The high heat value (HHV) of hydrogen production is 39.4 kWh per kg H_2. The energy consumption of an alkaline electrolyzer can be converted to an HHV-based efficiency of 79%. In addition, a pressurized electrolyzer needs more power consumption. Table 1 lists the specifications and operating parameters of alkaline electrolyzers [8,12–13]. The partial load operation of an AEC is limited to a range of 20%–40%, less than when the cell is poorly operational. The cell response to startup, shutdown, and load transition is also slow. These issues are associated with behaviors of the product gases that are supersaturated in the surrounding liquid electrolyte and form bubbles at the active sites of the electrode surface. The gas bubble behavior has a vital impact on the cell performance, especially when the load level is varying. This is a major challenge for applications with renewable power sources. It is therefore essential to reduce the polarization and dynamic barriers by optimizing the electrode–electrolyte interface [14].

Great efforts are being made to design zero-gap electrolyzers, as schematically represented in Fig. 2(b), with anion

Table 1. Specifications and operating parameters of alkaline and PEM electrolyzers [8,12–13]

Maturity	AECs	PEMECs
Current density / (A·cm^{-2})	0.2–0.4	0.6–2.0
Cell area / m^2	<4	<0.3
Hydrogen output pressure / MPa	<3	<3
Operating temperature / °C	60–80	60–80
Minimum partial load range / %	20–40	5–10
Overload (nominal load) / %	<150	<200
Ramp-up from minimum load to full load / (%·s^{-1})	0.13–10	10–100
Startup time from cold to minimum load	20 min–several hours	5–15 min
H_2 purity / %	>99.5	>99.99
Voltage efficiency (HHV-based) / %	62–82	68–82
Indicative system cost / (€·W^{-1})	1.0–1.2	1.9–2.3
System size range	0.25–760 Nm^{-3}·h^{-1}; 1.8–5300 kW	0.01–240 Nm^{-3}·h^{-1}; 0.2–1150 kW
Lifetime stack / h	<90000	<20000

exchange membranes (AEMs) [15]. The electrodes are in direct contact with the AEM surface, similar to that in proton exchange membrane fuel cells (PEMFC). In this way, the ohmic loss between electrodes will be minimized. Pure water, rather than aqueous alkali hydroxide solutions, is used as the feeding liquid without a corrosive electrolyte. A high AEM cell performance of 2.7 $A \cdot cm^{-2}$ at 1.8 V has been reported using a pure water electrolyte [16]. Construction of zero-gap cells requires stable and robust polymer membranes with a high OH^- conductivity to achieve operation at a current density above 1 $A \cdot cm^{-2}$. AEMs with imidazolium functionalized or sulfonated poly(ether ether ketone) backbones are desirable candidates to resist severe electrolyte attack [17]. Further efforts are needed to improve the ionic conductivity and durability of AEMs and ionomers.

2.2. Proton exchange membrane electrolysis cells

2.2.1. Cell construction and key materials

PEMECs, which are typically based on perfluorosulfonic acid, e.g., Nafion® membranes, are constructed with a solid proton-conducting membrane as an electrolyte. The membrane functions as a separator of the two electrodes and gases, and it has high proton conductivity, good mechanical strength, low gas permeability, and chemical stability. The construction of a PEMEC is schematically shown in Fig. 3. In contrast to AECs, the hydrogen product does not need to be purified. Porous electrodes loaded with catalysts are attached on each side of the membrane, i.e., in a zero-gap assembly. Electrode reactions in PEM electrolysis are written as:

$$\text{Cathode: } 2H^+ + 2e^- \rightarrow H_2,\ E^0 = 0\ \text{V} \quad (4)$$

$$\text{Anode: } H_2O \rightarrow \frac{1}{2}O_2 + 2H^+ + 2e^-,\ E^0 = 1.229\ \text{V} \quad (5)$$

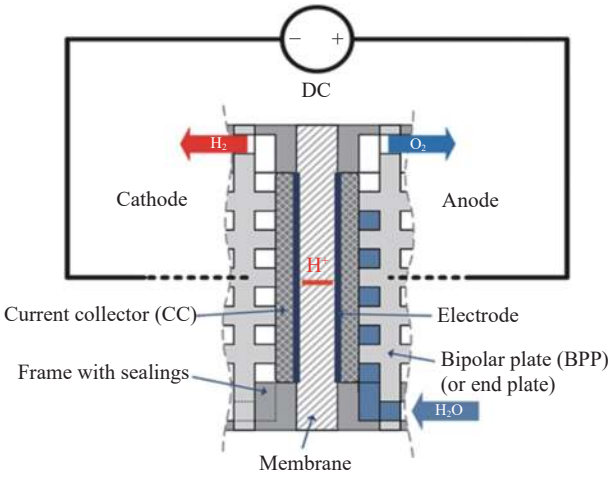

Fig. 3. Schematic of the construction of a PEMEC. DC represents direct current.

The selection of the acidic membrane electrolyte dictates the electrocatalyst and structural materials chosen from highly corrosion-resistant candidates. Active and stable electrocatalysts are limited to precious group metals (PGM), e.g., Pt or Pt/Pd alloy, as the hydrogen evolution catalysts at the cathode [18]. The state-of-the-art electrocatalyst for oxygen evolution is IrO_2 or IrO_2/RuO_2 with typical mass loadings of approximately 2 $mg \cdot cm^{-2}$ [19–20]. Iridium is a scarce element with a crust abundance of only 3×10^{-6} ppm and a global annual production of 7 t.

To store solar/wind energies, the worldwide installation of water electrolyzers requires a power capacity of several terawatts (1 TW = 10^{12} W), which can be translated to a hydrogen production rate over 10^7 t H_2 per hour. At a power density of 4 $W \cdot cm^{-2}$ and a catalyst loading of 2 mg Ir per cm^{-2}, state-of-the-art technologies need 1250 tons of Ir per TW^{-1}. In other words, the world's annual production of iridium would allow for a PEMWE installation of a few gigawatts capacity. A significant reduction of the iridium usage and eventual replacement of the metal must be realized for the commercial application of the technology in association with renewable energy storage.

On a technology level, these catalysts cover a small fraction of the stack (<10%) and system (<5%) cost. Because of the extremely corrosive conditions of PEMECs, i.e., the acidity of the electrolyte and the high potential of the anode, the use of carbon or stainless steel materials as cell components is excluded. Titanium is the most commonly used material for (anodic) porous transport layers and bipolar plates of PEMECs. Titanium forms an oxide surface layer, which is the primary cause of the performance deterioration. Stainless steel coated with Ti, Pt, Au, or carbon-based composites has been extensively explored as construction materials. These materials currently account for approximately 2/3 of the stack cost [8]. Even though prominent cost reductions have been achieved in recent years, significant efforts are needed to improve these components in terms of durability performance and material and processing costs.

2.2.2. Performance and challenges

The cell voltage and energy efficiency of PEMECs are 1.8–1.9 V and 78%–82%, respectively, at a current density of 1–2 $A \cdot cm^{-2}$ [20]. Table 1 lists a set of specifications and operating parameters of PEMECs. PEMEC is a technology that can operate in a partial load range, operational at a load level as low as 0–10%. As a result, PEMECs are a potential technology for use with renewable power sources. Considerable efforts are being made to demonstrate the technical feasibility of PEMECs in the renewable energy chain.

2.3. Solid oxide electrolysis cells

High operating temperatures of SOECs favor the kinetics of electrode reactions. SOECs can work near the thermoneutral point where the energy efficiency is as high as 100%. In principle, it is also possible for SOECs to achieve energy efficiency over 100% when they are integrated with other high-temperature devices (nuclear reactors, solar power, or combustors) to supplement thermal energies.

SOECs were initiated from solid oxide fuel cells (SOFC) technologies, i.e., using the materials available for SOFCs [21–22]. The typical electrolyte is yttria-stabilized zirconia (YSZ) with oxide ion conductivity. In addition, the solid electrolyte can also be proton conductive like $SrZr_{0.9}Yb_{0.1}O_{3-\delta}$

and $BaCe_{0.5}Zr_{0.3}Y_{0.2}O_{3-\delta}$. In $BaCe_{0.5}Zr_{0.3}Y_{0.2}O_{3-\delta}$, the corresponding electrode reactions of SOEC are the same as those of the PEM electrolyzer. Sr-doped $LaMnO_3$ (LSM) or $La_{0.6}Sr_{0.4}Co_{0.2}Fe_{0.8}O_{3-\delta}$ perovskite oxides serve as the anode, while porous cermet made of Ni-based alloys is used as the cathode.

For an oxide ion conductive electrolyte, the cell reactions can be written as follows:

$$\text{Cathodic reaction: } H_2O \rightarrow H_2 + O^{2-} + 2e^- \quad (6)$$

$$\text{Anodic reaction: } O^{2-} + 2e^- \rightarrow \frac{1}{2}O_2 \quad (7)$$

The SOEC performance generally degrades faster than that of SOFCs, creating challenges in developing SOECs with high performance and good durability [23]. Most of the degradation comes from the electrolyte, cathode, and anode. The YSZ electrolyte may degrade at the electrode interface, and the degrading mechanisms are classified as intergranular fracturing, grain boundary widening/coarsening, or void formation. Cathode degradation may occur via the agglomeration of Ni particles in the dense Ni–YSZ layer of the electrode. Delamination of the oxygen electrode–electrolyte interface is the major issue, depending on the oxygen-release ability of the oxygen electrode and electrolyte [24]. Thus, interface stabilization is required to prevent delamination by promoting the ionic conductivity of both the electrolyte and oxygen electrodes. In addition, the performance will further deteriorate because of the poisoning effects of the contaminants deposited from borosilicate glass sealant or Fe–Cr metallic alloys [25].

3. Hydrogen storage

Table 2 lists the selected physical properties of hydrogen as an energy carrier together with other types of liquid and gaseous fuels. Hydrocarbon fuels, such as petroleum and natural gases, are regarded as a source of hydrogen via reforming, although they are typically used as fuels for combustion. Methanol and ethanol are potentially renewable and used via direct oxidation or fuel reforming.

Table 2. Selected properties of hydrogen and other fuels

Fuel	Molar mass / ($g \cdot mol^{-1}$)	Freezing point / °C	Boiling point / °C	Mass energy density / ($MJ \cdot kg^{-1}$)		Density / ($kg \cdot L^{-1}$)		Storage pressure / MPa	Volume energy density / ($MJ \cdot L^{-1}$)		
				High heat value	Low heat value	Liquid	Gas at 0.1 MPa		Liquid	Gas at 0.1 MPa	Compressed gas
Hydrogen (H_2)	2.016	−259.2	−252.8	141.8	120	77	0.00008	70	10.1	0.011	5.6[b]
Methane (CH_4)	16.04	−182.5	−161.5	55.5	50.1	425	0.00066	25	25.2	0.036	9.0[c]
Ammonia (NH_3)	17.03	−77.7	−33.4	22.5	18.8	674	0.00073	0.1	11.6	—	—
Methanol (CH_3OH)	32.04	−98.8	64.7	22.7	19.8	786	—	0.1	17.8	—	—
Ethanol (C_2H_5OH)	46.07	−114.1	78.3	29.7	26.8	789	—	0.1	21.2	—	—
Gasoline[a] (C_4–C_{12})	60–150	−55–−70	<210	~45	~42	720–775	—	0.1	~33	—	—
Diesel[a] (C_4–C_{12})	150–250	−8–−12	<350	~46	~43	820–840	—	0.1	~35	—	—

Note: [a] Gasoline and diesel are mixtures of hydrocarbons with various compositions; [b] this number is based on a hydrogen tank at 70 MPa; [c] this number is based on a natural gas tank at 25 MPa.

The energy content of a fuel is defined as the volume-specific energy density ($MJ \cdot L^{-1}$) and mass-specific energy density ($MJ \cdot kg^{-1}$). The energy content can be calculated from either the HHV or low heat value (LHV) of the enthalpy changes ($\Delta H°$, $kJ \cdot mol^{-1}$) of hydrogen combustion depending on the state of the produced water (liquid or vapor).

Hydrogen has the largest energy density of all listed fuels on the basis of mass (141 $MJ \cdot kg^{-1}$); however, the lowest volume-specific energy density is in the form of either liquid or gas. The compressed hydrogen is often of engineering significance. Therefore, critical challenges for a hydrogen-based energy system are if it is compact and economical, and has safe storage.

Various hydrogen storage technologies have been developed or are under active development, and they can be categorized into (1) (cryo-)compression, (2) absorption or adsorption, or (3) chemical bonding via hydrides, amines/amides, hydrocarbons, or alcohols. Alternatively, the technologies can be grouped into the storage of elemental hydrogen or hydrogen carriers in porous, metallic, organic, or inorganic materials, as shown in Fig. 4.

3.1. Physical storage of elemental hydrogen

Physical hydrogen storage, e.g., compressed gas (CGH_2) and liquid (LH_2), is the most mature technology.

3.1.1. Compressed gas

Compressed hydrogen is an effective, simple, and state-of-the-art method for storing gas. All hydrogen-powered cars and busses use hydrogen as compressed gas. Physical compression is effective for increasing the energy density of hydrogen. Fig. 5 shows the density of hydrogen gas as a function of temperature at different pressures [26]. Low temper-

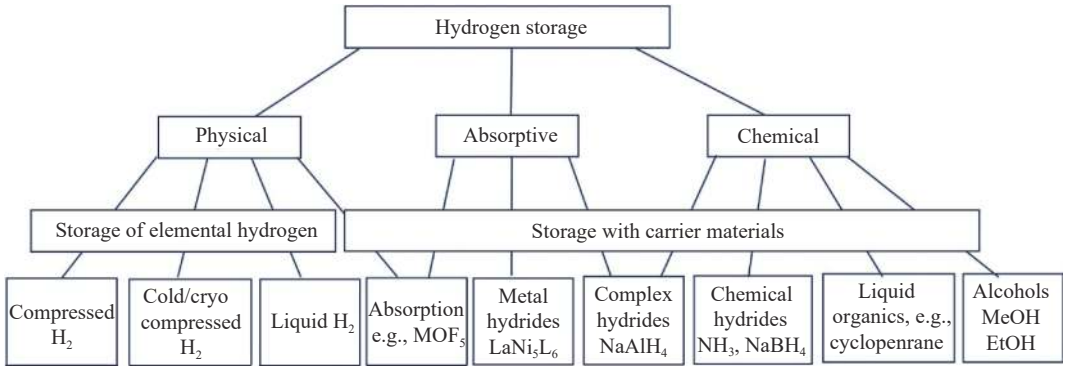

Fig. 4. Overview of hydrogen storage technologies.

atures and high pressures or combinations of the two parameters are commonly required for the high-density storage of hydrogen gas. The practical density of hydrogen gas is 11–50 $kg \cdot m^{-3}$ [27–28]. Four temperature–pressure regimes are identified: (a) compressing hydrogen at pressures up to 70 MPa and near ambient temperature; (b) coldly compressing hydrogen at high pressures up to 50 MPa and temperatures between 150 and 273 K; (c) cryo-compressed hydrogen at pressures up to 35 MPa and temperatures below 150 K; (d) liquefied hydrogen at pressures up to 0.6 MPa and temperatures near the boiling point ($T \approx 20$ K).

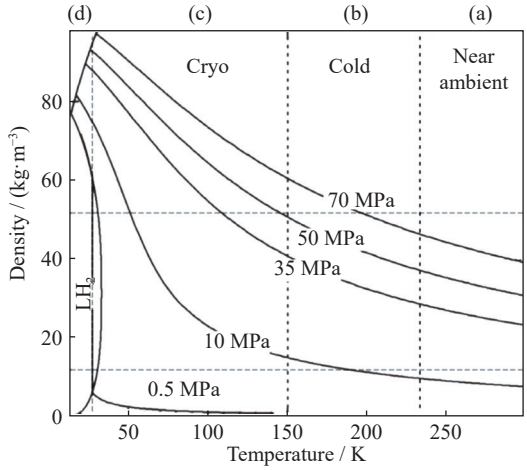

Fig. 5. Hydrogen density versus temperature for different storage pressures [26]. The horizontal dashed lines indicate the practical hydrogen density range, and the vertical dashed lines indicate the optional temperature–pressure regimes represented by (a) to (d). Adapted from *Compendium of Hydrogen Energy*, N.T. Stetson, S. McWhorter, and C.C. Ahn, Introduction to hydrogen storage, 3-25, Copyright 2016, with permission from Elsevier.

From a material point of view, few metals are impermeable to hydrogen. Fig. 6 shows the classification of tanks for hydrogen storage. Aluminum is widely used for small tanks at low pressures. Common laboratory 50 L cylinders made of steel are used for pressures up to 20 MPa, as shown in Fig. 6(a) and (b). These metal tanks, called Types I and II as, have a hydrogen content of less than 1% of the tank mass, and hence are prohibitively heavy for any automobile use. High-strength glass or carbon fiber composites, with or without metal liners, are generally used for hydrogen tanks of 35–70 MPa (Types III and IV as shown in Fig. 6(c) and (d)). At such high pressure, hydrogen storage content over 5.0wt% H_2 with an energy density as high as 5.0 $MJ \cdot L^{-1}$ can be achieved [29]. Recently, overwrapped pressure vessels based on metal- or polymer-lined carbon fiber composites were developed for transport and stationary storage, offering a high payload capacity greater than 1000 kg hydrogen [30–33]; however, cost and safety issues should be further assessed.

Hydrogen storage can be further densified by decreasing the temperature, as clearly shown in Fig. 5. Cold- and cryo-compression have been explored as approaches toward on-board hydrogen storage at a higher density regarding mass and volume. A 48.2 kg Type IV cylinder stored 5.6 kg hydrogen at 50 MPa and 200 K, introducing a 45% mass reduction for a 70 MPa analog cylinder under ambient temperature [34]. By further reducing the compression temperature to 80 K, the storage capability was enhanced from 5 kg (at 298 K and 70 MPa) to 16.5 kg (at 80 K and 70 MPa) [26]. In the

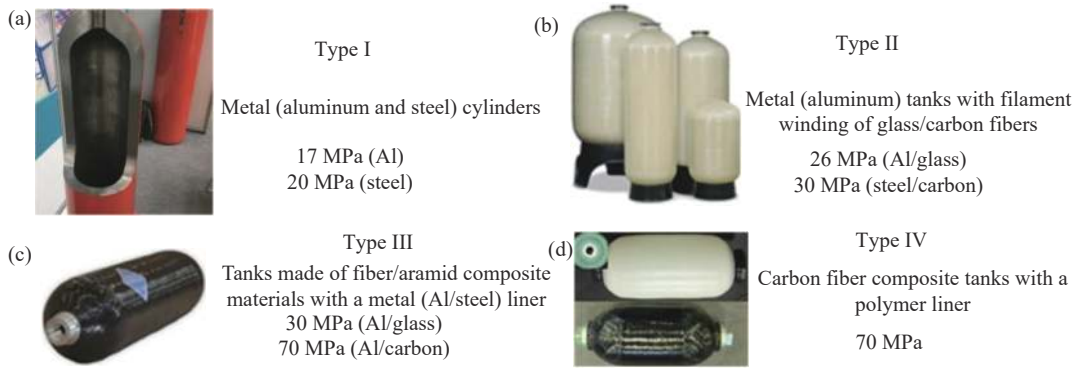

Fig. 6. Classification of hydrogen storage tanks: (a) Type I; (b) Type II; (c) Type III; (d) Type IV.

cryo-compression case, the storage vessel should be designed with vacuum insulation to keep the low temperature as well as a sufficiently high-pressure resistance. An advanced cryo-compressed cylinder is made of a composite inner surrounded by vacuum space filled with numerous layers of multilayer insulation and then a metallic jacket, as schematically shown in Fig. 7(a) [26]. The insulated pressure cylinders are then able to share the compact advantages of liquid hydrogen and the ambient temperature of the compressed hydrogen. However, this should increase the hydrogen storage system cost because of the additional cylinder requirements.

In addition, for the purpose of hydrogen market supply with seasonal fluctuations, large scale and long-time storage underground have been investigated, e.g., depleted oil, gas reservoirs, or salt caverns [35–37]. Underground pipes are an economical option for high storage capacities, e.g., over 20 tons and operational at pressures over 10 MPa. The current technologies for underground hydrogen storage are still immature, despite several practical cases in the USA and Europe.

3.1.2. Liquid hydrogen

Hydrogen has a normal (under 1 atm pressure) boiling point of 20.4 K, at which liquid hydrogen has a density of 71 $kg \cdot m^{-3}$ or $g \cdot L^{-1}$. Some gases, such as propane, butane, and ammonia, can easily be liquefied by compression at room temperature (RT). However, that is not the case for hydrogen, where the molecular interactions are very weak. As a result, the critical temperature of hydrogen is approximately 33 K. Only at temperatures less than this critical point can hydrogen be liquefied. The process has been exploited on a large scale; for example, the National Aeronautics and Space Administration (NASA, USA) has constructed liquid hydrogen vessels with capacities of up to 270 metric tons, as shown in Fig. 7(b) [38–40].

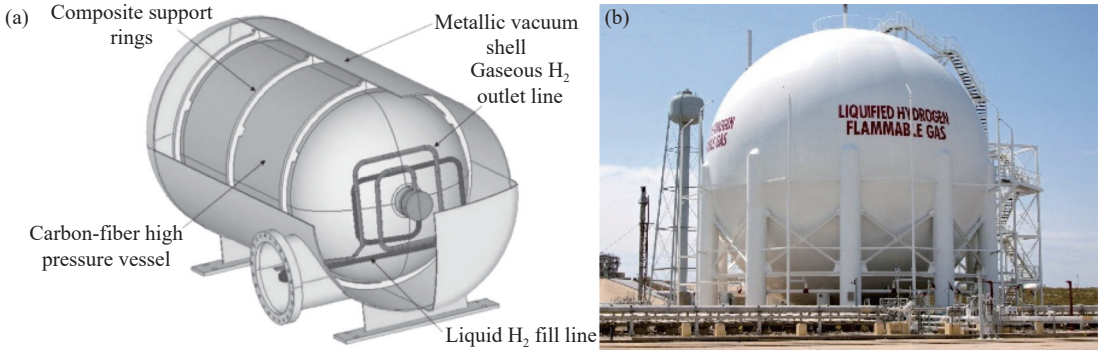

Fig. 7. (a) Schematic of a cryo-compressed hydrogen storage vessel [26]. (b) Liquid hydrogen tank system [38]. (a) Reproduced from *Compendium of Hydrogen Energy*, N.T. Stetson, S. McWhorter, and C.C. Ahn, Introduction to hydrogen storage, 3-25, Copyright 2016, with permission from Elsevier. (b) Reproduced from *Int. J. Hydrogen Energy*, 46, R.R. Ratnakar, N. Gupta, K. Zhang, C. van Doorne, J. Fesmire, B. Dindoruk, and V. Balakotaiah, Hydrogen supply chain and challenges in large-scale LH2 storage and transportation, 24149-24168, Copyright 2021, with permission from Elsevier.

Technically, cooling is achieved by throttling liquid nitrogen. The average heat capacity of hydrogen for the cooling interval and heat of condensation at 20 K are 28.5 $J \cdot mol^{-1} \cdot K^{-1}$ and 892 $J \cdot mol^{-1}$, respectively. The primary issue for LH_2 storage is the energy-intensive liquefaction process, consuming approximately 1/3 the LHV of the stored hydrogen, i.e., 30–45 $MJ \cdot kg^{-1}$ of 120 $MJ \cdot kg^{-1}$ [41]. Another issue is the boil-off loss of hydrogen because of heat leakage through the storage vessel walls, which wastes energy liquefying hydrogen and requires relief valves to vent the evaporated gas from inside the vessel. This is critical when the storage period of liquid hydrogen is long. Despite the need for (thermal) insulation, liquid hydrogen storing vessels are less expensive than cylinders for compressed hydrogen gas per weight of stored hydrogen [35–36]. Liquid hydrogen storage is not a practical solution for fuel cell-driven motors; however, it may be a potential candidate for applications requiring high volume and dense storage without concern for the boil-off (e.g., commercial aircraft).

3.2. Hydrogen storage with carrier materials

Hydrogen storage with carrier materials offers denser storage than either physical or chemical bonds to the host materials [42]. In addition to the hydrogen capacity (mass ratio of the host materials), the thermodynamics and kinetics for the uptake and release of hydrogen are fundamental. The carrier materials can be classified as adsorbents, metal hydrides, organic liquids, or synthetic fuels.

3.2.1. Adsorbents

Hydrogen storage using porous materials has been investigated at safe pressures and near ambient temperatures. The adsorbents generally have a large specific surface area, storing hydrogen via physical van der Waals bonding at high pressures and low temperatures. These porous materials include metal–organic frameworks (MOFs), porous polymeric materials, porous carbon-based materials, and zeolites [40], as listed in Table 3. Advanced carbon materials, e.g., carbon nanotubes and carbon nanofibers, are research hotspots for hydrogen adsorption. Up to 5wt% H_2 can be adsorbed on rigid porous carbons under high pressures at −196°C. A linear correlation has been established between H_2 storage capacities at 77 K and the specific surface areas of the various MOF materials. At a Brunauer-Emmett-Teller (BET) surface area of 6000 $m^2 \cdot g^{-1}$, hydrogen uptake of nearly 10wt% has been

Table 3. Sorption properties of hydrogen on different types of adsorbents

Class	BET surface area / ($m^2 \cdot g^{-1}$)	Maximum storage capacity / wt%	
		At RT	At 77 K
Carbon materials	700–3000	0.6	5
Zeolites	700	0.1	2
MOFs	6000	1	9
Polymers	1900	0.5	3.7

demonstrated at 77 K and up to 100 atm. However, these numbers are reduced to approximately 1wt% at ambient temperature, which is too low for practical use.

3.2.2. Metal hydrides

Hydrogen bonds with metals and alloys, forming hydrides, have been extensively and continuously investigated as hydrogen storage materials [36,43–45]. In fact, the hydrogen storage density of metal hydrides has a practical range, e.g., 6.5 atom H per cm^3 for MgH_2. Thus, they could be regarded as potential hydrogen carriers with high hydrogen capacity per unit volume or mass.

The hydrides can be categorized as interstitial compounds or chemical compounds. The interstitial compound refers to when hydrogen atoms stay in the interstitial hole of a host metal lattice, while hydrogen atoms can also chemically bond with the host metal. In general, hydrogen bonding and release are reversible in the interstitial compound under moderate pressure and temperature. The most studied interstitial hydrides include MgH_2, Mg_2NiH_4, and $NaAlH_4$, as listed in Table 4. Hydrogen in metal hydrides is stable, and its release requires high energy.

Simple binary hydrides, such as MgH_2 and AlH_3, are of special interest. Magnesium is abundant, relatively inexpensive, and light, and MgH_2 reversibly stores 7.6wt% hydrogens [44]. However, MgH_2 is quite stable, and the hydrogen desorption temperature is greater than 300°C for a 0.1 MPa plateau pressure [46].

Table 4. Hydrogen storage properties of select metal hydrides

Metal hydrides	Reversible capacity / (wt% H_2)	Heat of desorption / (kJ per mol H_2)	Desorption temperature at 1 atm / °C
Interstitial hydrides	1–2	Circa 30 (ca. 12.4% LHV)	RT
Binary hydrides (MgH_2)	7.6	74.5 (30.8% LHV)	300
Intermetallic hydrides (Mg_2NiH_4)	3.6	64.5 (26.7% LHV)	255
Complex hydrides ($NaAlH_4$)	3.7	37 (15.3% LHV)	150

Intermetallic hydrides form at near ambient conditions; for example, $LaNi_5H_6$ is the most studied material. The host metal alloys typically contain a metal (A) with high affinity for hydrogen and a metal (B) with low affinity. A large family of intermetallic hydrides is available and often grouped by the atomic ratio of the two metals. The most studied types are AB_5 (e.g., $LaNi_5H_6$) and AB_2 (e.g., Mg_2NiH_4), with a typical hydrogen storage capacity of 1wt%–2wt% [28,40]. This capacity is low for hydrogen storage in automobile applications where a storage of 4–5 kg H_2 is desired.

The search for hydrides with higher hydrogen content focuses on compounds with lighter elements of periods 2 and 3 (from Li and Na). These light elements do not form interstitial hydrides; however, they develop a class of complex hydrides with a center anion AlH_4^- (alanates) and BH_4^- (borohydrides) that are typically balanced by light metals. Complex hydrides exhibit high hydrogen content; for example, $NaAlH_4$ has a hydrogen content of 7.5wt%, and $Mg(BH_4)_2$ has a hydrogen content of 14.8wt% [45]. The sodium alanate decomposes in several steps:

$$3NaAlH_4 \rightleftharpoons Na_3AlH_6 + 2Al + 3H_2 \rightleftharpoons 3NaH + 3Al + 9/2H_2 \rightleftharpoons 3Na + 3Al + 6H_2 \quad (8)$$

In the first step, 3.7wt% hydrogen is liberated, and the more stable hexahydride, Na_3AlH_6, is formed, which in the following step liberates 1.85wt% more hydrogen with the formation of NaH. This produces a practical hydrogen content of 5.6wt% H_2 out of the total 7.4wt% content. The last 1.9wt% H_2 in $NaAlH_4$ remains as NaH, which is a completely irreversible chemical hydride such as LiH, CaH_2, and $NaBH_4$. The word "irreversible" means that the release of the remaining hydrogen requires a significantly higher temperature and the use of alkali metals. After the hydrogen is released, these hydrides can only be recharged via chemical pathways. In other words, more energy input is demanded, similar to other types of chemical hydrogen carriers, such as alcohols or hydrocarbons, which will be discussed in the following sections.

3.2.3. Organic liquids

Liquid organic hydrogen carriers (LOHCs), such as N-ethylcarbazole and dibenzyltoluene [47], have been investigated because of the reversible hydrogen storage and release in the liquid state. LOHCs differ from organic fuels because they are regenerative as hydrogen carriers. The principle is that the double bonds in the aromatic (double-bonded) structures are saturated with hydrogen on the charge, and the process is reversed when hydrogen is liberated, as exemplified with N-ethylcarbazole [48].

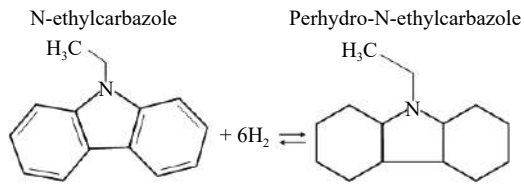

(9)

N-ethylcarbazole is a solid (melting point 68°C), and approximately 10% more dehydrogenation product, perhydro-

N-ethylcarbazole (melting point < 20°C), is typically added to maintain the liquid state. The resulting hydrogen storage capacity of 5.8wt% is reduced by 90%. Hydrogenation and dehydrogenation are carried out over a catalyst of either noble or non-noble metals. The hydrogenated form of the LOHCs is kinetically stable at ambient conditions; the hydrogenated LOHCs are passed over a catalyst at the decomposition temperature, and hydrogen is liberated when dehydrogenation is desired. In general, dehydrogenation reactions need to be thermally activated at temperatures greater than 200°C. Moreover, hydrogen liberation is an endothermic process, and reaction enthalpies of 50–70 kJ per mol H_2 are common.

3.2.4. Synthetic fuels

Synthetic fuels include carbonaceous fuels (hydrocarbons, alcohols, etc.) and nitrogen-containing fuels (ammonia and hydrazine). The common feature of these fuels is that they are synthesized from H_2. The chemical energy built into these fuels originates from hydrogen, which is potentially sustainable in association with renewable energies. These fuels can also be produced by thermochemical processes or fermentation of biomass, and they have been considered as hydrogen carrier candidates [49]. A major advantage of these compounds is the direct use of current chemical infrastructure for production, storage, and delivery. Furthermore, hydrogen delivery in the form of liquids can be of high capacity without high pressures. The use of hydrocarbon liquids (e.g., methanol and formic acid) as hydrogen carriers can realize net-zero carbon emission because it establishes a carbon cycle of capturing, storing, and recycling associated with the hydrogen storage and release. However, the energy efficiencies of such hydrogen carriers should be considered.

3.3. Hydrogen transportation and refilling

The world's annual hydrogen production is more than 100 million metric tons. The hydrogen infrastructure is being developed with two main topologies, massive production at a central site followed by second distribution to hydrogen refueling stations and local production using small-scale apparatus. Distribution to retail stations is accomplished via tankers by road, rail, or ship at pressures around 20–50 MPa [50]. Liquid hydrogen can also be transported using tube trailers with strict regulations [51]. Overseas transportation of hydrogen was initialized by Europe-Quebec and Japan during the 1980s and 1990s [52].

By the end of 2020, there were 540 hydrogen refilling stations worldwide, supporting approximately 35000 fuel cell vehicles. Of these, approximately 50% of the refilling stations and 65% of the fuel cell vehicles are in Asia (Japan, China, and Korea) [53]. The current investment cost of hydrogen refilling stations is estimated to be 1.2–2.0 million euros, depending on the daily dispensing capacity and onsite/offsite hydrogen production [54].

4. Fuel cells for electrochemical energy conversion

4.1. Electrochemical versus chemical devices

Electrochemical energy conversion is key to future energy systems using hydrogen as the energy carrier. This includes the electrochemical production of hydrogen via electrolysis, electrochemical conversion of hydrogen to power, and other power to fuel (PtX) processes [49]. Conventionally, the energy conversion route from fuel to power is accomplished via chemical combustion (from chemical energy to heat), thermal engines (from heat to mechanical energy), and electrical generators (from mechanical to electrical energy). The energy conversion efficiency of modern power plants is less than 40%, with 10%–20% for small engines [55–56]. Another critical issue is the energy production from fossil fuels promoting greenhouse gas emissions.

A fuel cell can directly convert the chemical energy in fuels (e.g., H_2 gas) to electricity via electrochemical reactions. The principle of a hydrogen–oxygen fuel cell is illustrated in Fig. 8, where either a proton or an oxide electrolyte is adopted. Hydrogen must be separated from oxygen using a dense electrolyte to avoid direct chemical reduction of H_2 gas. The electrolyte is a unique material that is able to conduct ions, such as protons or oxides (O^{2-}), instead of electrons. Hydrogen is catalytically oxidized at the anode (negative), while oxygen is reduced at the cathode (positive). The electrolyte makes the electrons flow from anode to cathode via the external circuit, i.e., generation of the electrical power. The half-cell reactions at the anode and cathode de-

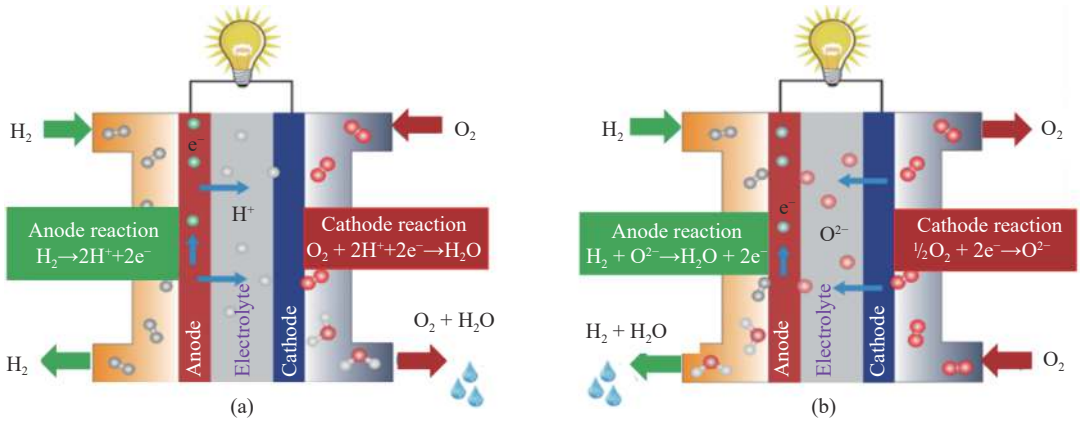

Fig. 8. Schematic of fuel cell principles based on a (a) proton-conducting electrolyte and (b) oxide-conducting electrolyte.

pend on the charge carrier through the electrolyte; however, the overall reaction is the same (E^0_{cell} is the standard cell potential).

$$1/2O_2 + H_2 \rightarrow H_2O,\ E^0_{cell} = 1.23\ V \quad (10)$$

The open-circuit voltage of a fuel cell can be calculated from the Gibbs free energy change ($\Delta G^{\ominus}$) of the cell reaction, which at room temperature and under standard pressure conditions is:

$$E^0_{cell} = \frac{-\Delta G^{\ominus}}{nF} = \frac{237200\ J\cdot mol^{-1}}{2\times 96485\ C\cdot mol^{-1}} = 1.23\ V \quad (11)$$

where n and F are electron number and faraday constant, respectively. As the value of the Gibbs free energy decreases (becoming less negative) with increasing temperature, so does the fuel cell open-circuit voltage. For example, at 800°C, the E^0_{cell} becomes 1.18 V under standard pressure conditions.

Electrochemical fuel cells have a higher intrinsic efficiency over conventional technologies because of the direct conversion of chemical energy into electricity. The energy conversion efficiency (η) of fuel cells is limited only by the ratio of the Gibbs free energy (ΔG) to the enthalpy (ΔH) of the cell reaction (ΔS is the entropy change):

$$\eta = \Delta G/\Delta H = 1 - \frac{T\Delta S}{\Delta H} \quad (12)$$

This expression has similarity to the Carnot efficiency (η_{max}), which is a function of the temperatures of the cold (T_C) and hot (T_H) sources:

$$\eta_{max} = 1 - \frac{T_C}{T_H} \quad (13)$$

The efficiency of fuel cells is dependent on the physical (gas or liquid) forms of the reactants and products, not on temperatures, as is the case with thermal engines. With the formation of liquid water (high heat value), this maximum fuel cell efficiency at room temperature can be as high as 94.5%, which becomes 83% if the water product is vapor (low heat value).

In contrast to internal combustion engines used in power plants or automobiles, the operation of fuel cells does not involve high-temperature combustion, which significantly minimizes the emission of air pollutants like SO_x, NO_x, and particulates when fossil fuels are used. When using pure hydrogen, the cell releases only water as the by-product and is, therefore, a zero-emission device.

From the viewpoint of energy conversion, a fuel cell clearly performs like a battery. Batteries store the reactants in electrodes or electrolytes and therefore have a limited capacity. Fuel cell electrodes are made of catalysts, while all reactants (oxidant and fuel) are supplied from the outside whenever power is required. The capacity of fuel cells is primarily restrained by the dimensions of the fuel tanks. When fuel is exhausted, it is able to be refueled quickly, similar to automobiles.

4.2. Types of fuel cells

Materials that can conduct H^+ and O^{2-}, OH^-, or CO_3^{2-} ions have also been selected as electrolytes for fuel cells. The fuel cells can be classified into several types according to the electrolyte used, i.e., alkaline fuel cells (AFCs), anion exchange membrane fuel cells (AEMFCs), phosphoric acid fuel cells (PAFCs), PEMFCs, molten carbonate fuel cells (MCFCs), and SOFCs. The electrolyte primarily dominates the working temperatures, electrode reactions, and materials, as well as the fuel cell operation and construction. Aqueous electrolytes fuel cells like AFCs and PAFCs operate at below 200°C while SOFC and MCFC function at temperatures greater than 600°C. Brief discussions on the classified fuel cells are listed below and summarized in Table 5.

(1) AFCs.

This kind of fuel cells uses the concentrated KOH electrolyte, and the working temperature ranges from RT up to 200°C. In AFCs, liquid KOH electrolyte is either circulated or fixed in a porous matrix. Various electrocatalysts have been selected for use, such as Ni, Ag, metal oxides, and noble metals. CO_2 from air or reformate fuel reacts with KOH to form K_2CO_3, which blocks electrode pores and changes the electrolyte. AFC, as the first developed modern fuel cell, was used as an onboard electricity source for the Apollo space missions. Nevertheless, further exploration of use on land is hindered by its low tolerance to CO_2. A solid alkaline AEM is a desirable candidate to substitute the liquid electrolyte, i.e., an AEMFC may have the combined advantage of AFC and PEMFC [57]. AEM is usually a polymer electrolyte with good anionic conductivity (OH^-). CO_2 poisoning can be greatly mitigated by inhibiting the precipitation of free carbonates. However, the potential carbonation decreases the anion conductivity of AEM [58].

(2) PAFCs.

100% H_3PO_4 (PA) is selected as an electrolyte in which CO_2 is completely inert. PAFCs usually use silicon carbide as a matrix to retain the acid because of the stability of silicon carbide in hot PA [59]. The working temperature of 150–220°C enables PAFCs to tolerate fuel impurity (CO) poisoning. In this temperature range, heat management, i.e., cooling, is less an issue for PAFCs. In addition, the waste heat can be recycled for cogeneration of heat and power. PAFCs have been successfully commercialized for stationary power units, e.g., PC-25 with a power capacity of 200 kW. Nevertheless, the highly corrosive PA greatly impacts the electrode materials (e.g., electrocatalysts) as well as the lifetime of the stack components.

(3) PEMFCs.

PEMFCs use an acidic electrolyte in the form of polymer membranes (e.g., perfluorosulfonic acid), which have high ionic conductivities greater than 0.1 $S\cdot cm^{-1}$. However, the working temperature is limited at ~80°C under such highly hydrated conditions. The most effective electrocatalyst for PEMFCs is platinum (Pt), which is scarce and costly, regardless of the recycling of Pt. Much has been done to decrease the use of precious metals by low metal loading, optimization of Pt alloys, and development of non-noble metal catalysts [60]. Challenges, such as water and thermal management at high current densities, are still critical to PEMFCs for

Table 5. Classification and characteristics of fuel cells

Fuel cells	Temperature / °C	Electrolyte (in matrix)	Charge carrier	Anode	Cathode	Bipolar plate	Primary fuel	Oxidant	Efficiency / %	Power size	Operating features	Applications	Notes
AFCs	40–80/ 200–260	Aqueous/molten KOH (asbestos/polymer /ceramic)	OH^-	Ni, metal oxides	Pt/C/NiO	Metal	H_2	O_2 (CO_2 scrubbed air)	45–60	1–100 kW	+ Fast cathode kinetics, cheap electrolyte, low-cost catalysts and stack materials. − Sensitive to CO_2 in both fuel and air, H_2 circulation, complex systems.	Military; space	Active development of anion exchange membrane
PEMFCs	40–80	Perfluorosulfonic acid	H^+ (H_3O^+)	Pt/C	Pt/C	Graphite/metal/ composite	H_2 (+ CO_2)	O_2/air	40–60	10 W–1 MW	+ Solid construction, high power density, low temperature, quick startup, fast load response. − Noble metal catalysts, water management, intensive cooling, low waste heat value, low CO tolerance.	Stationary and portable power; transportation; distributed generation	Active development of HT-PEMFC
PAFCs	180–210	H_3PO_4 (soaked in SiC)	H^+	Pt/C	Pt/C	Carbon composites	H_2 (+ CO_2 +1% CO)	Air	40–45	200–400 kW	+ CO tolerance (external CH_4 reforming), no water management, easy cooling, good heat value (CHP). − Sluggish ORR kinetics, noble metal catalysts, slow startup, low power density.	Distributed generation	—
MCFCs	600–650	Li–K(Na)CO_3 (soaked in $LiAlO_2$)	CO_3^{2-}	Ni alloy	Lithiated NiO	Stainless steel	H_2/CO	Air + CO_2	45–60	0.3–3 MW (300 kW module)	+ High efficiency, fuel flexibility (internal CH_4 reforming), non-noble metal catalysts, cheap stack materials, good heat value (CHP). − Large ohmic resistance, low current/power density, HT corrosion, slow startup.	Electric utility; distributed generation	—
SOFCs	600–1000	Y_2O_3–ZrO_2	O^{2-}	Ni/YSZ	LSM	Metal/ ceramic	H_2/CO	Air	60–65	1 kW–2 MW	+ Solid construction, high efficiency, solid construction, fuel flexibility (internal CH_4 reforming), nonnoble metal catalysts, good heat value (CHP). − HT corrosion, slow start.	Auxiliary power; electric utility; distributed generation	—

Note: +: positive attribute; −: negative attribute; CHP: combined heat and power; ORR: oxygen reduction reaction.

system construction and operation. In addition, the low tolerance to impurities, e.g., carbon monoxide in the fuel stream, is also of concern. Further efforts have been used to develop PEMFCs working at temperatures greater than 100°C.

(4) MCFCs.

MCFCs use alkali metal molten carbonates as the electrolyte, supported by a ceramic $LiAlO_3$ matrix [61]. The operating temperature is approximately 600–650°C, allowing the use of non-noble metal electrocatalysts such as Ni and NiO. Furthermore, the high temperature (HT) also has other advantages, including direct energy conversion of CO and CH_4 via internal fuel reformation. Use of the waste heat is also possible for improving the overall efficiency [61–62]. Stainless steel is most widely used to construct MCFCs. The main issues of MCFCs are material corrosion and a limited lifetime.

(5) SOFCs.

SOFCs are an all-solid device operating at 600–1000°C [63–64]. This high temperature range allows for a wide selection of catalysts and fuels via internal reforming. High energy efficiency and quality of waste heat make SOFCs capable of providing power from kW to MW for stationary and distributed applications. The typical electrolyte for SOFCs is a dense YSZ with sufficient oxide conductivity. Porous Ni and lanthanum strontium manganite (LSM) oxides are used as the anode and cathode, respectively [65–66]. The key issues for SOFCs are the thermal cycle capability, system controllability, and stack durability. The stack's durability greatly depends on the electrode materials. Reducing the working temperature to an intermediate range of 500–800°C, i.e., intermediate temperature (IT)-SOFCs, is a potential route to mitigate the issues mentioned above.

4.3. Construction of cells and stacks

In this section, PEMFC is used to illustrate the fuel cell construction. A single fuel cell consists of three components, a polymer electrolyte, anode electrode, and cathode electrode. When these components are assembled into a cell, it is often called a membrane electrode assembly (MEA) (shown in Fig. 9).

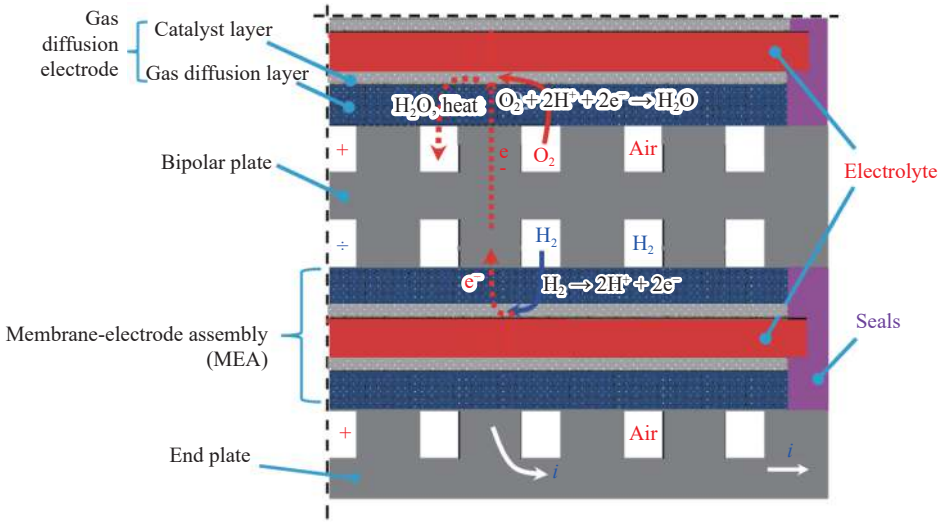

Fig. 9. Schematic of the PEMFC construction and stacking. *i* represents current.

The electrode is constructed with a porous gas diffusion layer on which a catalyst layer is applied. The resulting electrode is called a gas diffusion electrode (GDE), which is then sandwiched with a membrane to create an MEA. Alternatively, the catalyst layer can also be applied to the polymer membrane, and the obtained component is called the catalyst-coated membrane, which is then sandwiched with two pieces of gas diffusion layers during the fuel cell assembly.

Interconnection is required when multiple cells are stacked together. This interconnection should offer flow channels for both fuel gas and oxygen. Additionally, the interconnection also serves as the cathode and anode on the two sides. Thus, the interconnect is commonly called a bipolar plate that has high electrical and thermal conductivity, low gas permeability, high mechanical strength, and good corrosion resistance to harsh conditions in fuel cells.

In addition, a gas-tight seal and electrical insulation are also required by using ceramic fibers for high-temperature fuel cells or plastic gaskets for low-temperature fuel cells. Other components, such as a current collector and cooling plate/channel, are auxiliary in the fuel cell stack. A fuel cell power system also includes other equipment such as sensors, a gas humidifier, heat exchanger, pumps, and compressors. These other components are called the balance-of-plant, which account for ca. 50% of the system cost.

4.4. Proton exchange membrane fuel cells

4.4.1. Membrane electrode assemblies and materials

MEAs, consisting of three layers, including a porous gas diffusion layer, catalyst layer, and membrane [67], are the heart of the PEMFCs where the electrochemical reactions occur for power generation. Proton exchange membranes are usually poly(perfluorosulfonic acid), consisting of perfluorinated backbones on which the sulfonic acid groups are fixed. The backbones are hydrophobic, providing structural integrity and mechanical strength to the membrane, while the

acidic domain is hydrophilic, accommodating the absorbing water. PEM could solvate the protons and enable their passage. The cylindrical channels between ion clusters permit the hydrodynamic permeability of both charged and uncharged species [68].

Water uptake and swelling are key parameters for PEMs with proton conductivity. Under full hydration (100% relative humidity), the membranes exhibit an ionic conductivity of approximately 0.05–0.06 $S \cdot cm^{-1}$ at room temperature, which increases to greater than 0.1 $S \cdot cm^{-1}$ at approximately 80°C. The most widely used membranes are polytetrafluoroethylene fiber-reinforced composites with a thickness down to 10 μm, allowing for minimized ohmic resistance [69].

Carbon-supported Pt nanoparticles are state-of-the-art catalysts. The Pt particle size is 2–5 nm to compromise the specific activity and long-term stability [70]. It is a common practice to select Pt alloys, e.g., Pt_xNi, to achieve a promoted specific activity by 3–5 times, corresponding to an increase in the fuel cell voltage by approximately 40–50 mV. High specific surface area carbon blacks are essential to facilitating the dispersion and stability of metal nanoparticles. The carbon support is primarily graphene-like agglomerates with a size of 30–60 nm with a BET surface area from 10 to 1000 $m^2 \cdot g^{-1}$. Carbon-supported Pt catalysts with different metal contents from 10wt%–60wt% are commercially available [70]. At a fixed Pt loading of about 0.3–0.5 $mg \cdot cm^{-2}$, a higher metal content implies a thinner catalyst layer, beneficial for mass transport during the fuel cell operation [71].

GDEs have catalyst powders with an ionomer as a binder, which enables the protonic conductivity of the catalyst sites [72]. The gas diffusion layer (GDL), in the form of either paper or cloth, is mainly comprising carbon fibers with a diameter of ~7 μm, serving as a substrate to support catalyst particles. The GDL materials have a porosity up to 70%, with macropore sizes of 10–30 μm. To apply the carbon-supported catalyst with micropore sizes of 10–100 nm, an intermediate transition layer is needed, called a microporous layer. The microporous layer is usually made of carbon blacks (5%–30% loading) bonded with polytetrafluoroethylene (PTFE, Teflon®) to make the layer hydrophobic for the purpose of water removal during the fuel cell operation. The structure of the microporous and catalyst layers is schematically represented in Fig. 10.

4.4.2. PEMFC performance and challenges

A key to optimization of the fuel cell performance is to extend the three-phase boundary at the interface between the catalyst layer and membrane where both electrode reactions occur. With a Pt loading of 0.3–0.5 $mg \cdot cm^{-2}$, corresponding to a catalyst layer of ca. 10-μm thick, PEMFC may achieve a state-of-art performance, e.g., a power density of 0.75 $W \cdot cm^{-2}$ at a current density of 1 $A \cdot cm^{-2}$. Correspondingly, the metal consumption is estimated at approximately 0.19 $g \cdot kW^{-1}$, accounting for 53% of the MEA cost. The cost, activity, and stability of the noble metal (Pt) catalysts are the most critical challenges to the PEMFC technology.

4.5. Solid oxide fuel cells

4.5.1. SOFC structures and materials

SOFCs are based on ceramic electrolytes, e.g., dense YSZ, operating at high temperatures (600–1000°C) [63]. The ceramic electrolyte is sandwiched by two porous electrodes. The main electrochemical reactions at the anode and cathode are described as follows:

$$\text{Anode: } H_2 + O^{2-} \rightarrow H_2O + 2e^- \quad (14)$$

$$\text{Cathode: } 1/2O_2 + 2e^- \rightarrow O^{2-} \quad (15)$$

$$\text{Overall: } 1/2O_2 + H_2 \rightarrow H_2O \quad (16)$$

The total reaction combines hydrogen and oxygen, forming water vapor. In particular, oxygen at the cathode gains free electrons from the external circuit to form O^{2-}. The charged oxygen ions move to the anode via the ceramic elec-

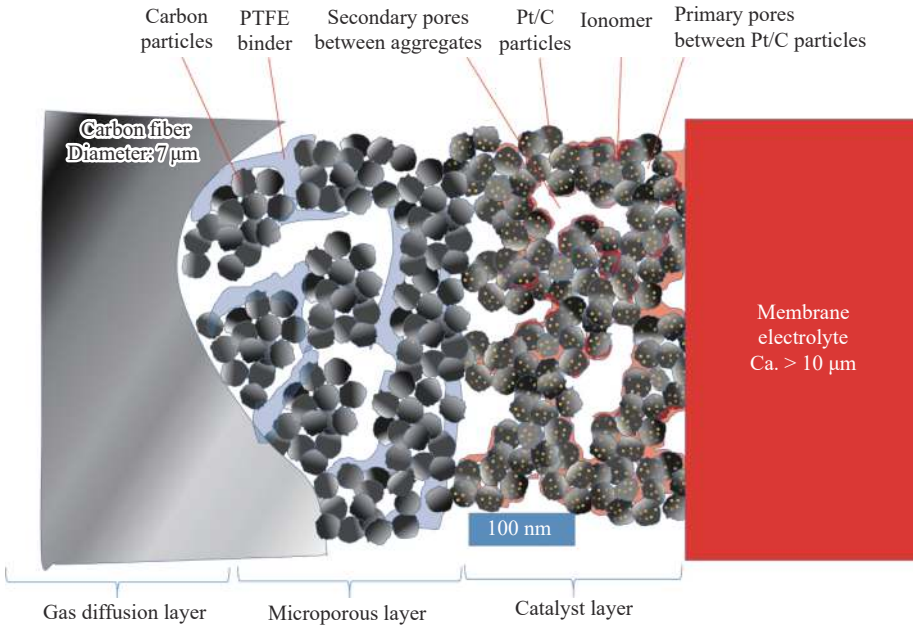

Fig. 10. Schematic representation of the MEA structure of a PEMFC.

trolyte and react with the hydrogen from the fuel stream, simultaneously producing electricity and water vapor. Apart from pure hydrogen, hydrocarbons, carbon monoxide, or ammonia can be used as fuel for SOFCs. This is of great significance for carbon neutrality because the so-called biohydrogen, biogas, and biohythane (produced from the anaerobic digestion of organic wastes) consisting of hydrogen, methane, carbon dioxide, and water are suitable fuels for SOFCs [73]. However, fuel reforming is necessary for the electrochemical energy conversion of methane. The fuel reforming reactions convert a less active fuel into a more active fuel, described as follows:

$$CH_4 + 2H_2O \rightarrow 4H_2 + CO_2 \quad (17)$$

$$CH_4 + CO_2 \rightarrow 2H_2 + 2CO \quad (18)$$

$$CO + H_2O \rightarrow H_2 + CO_2 \quad (19)$$

Alternatively, SOFCs have drawbacks including high cost, low fuel efficiency, and poor robustness in terms of startup and thermal/load cycling. The crucial working conditions create great challenges for electrodes and stack materials. For example, electrodes and stack materials should be highly heat resistant and conductive to provide sufficient interfaces for electrochemical reactions and freely conduct the electrons to an external circuit. Continuous efforts have been made to overcome these challenges.

The ceramic electrolyte in SOFCs functionally transports oxygen ions from the cathode to the anode and separates the two electrodes with good electronic isolation. YSZ, as an electrolyte for SOFCs, offers high ionic conductivity (around 0.01–0.1 $S \cdot cm^{-1}$) as well as the desired chemical and mechanical stability at high temperatures (800–1000°C) [65–66]. Gadolinium-doped ceria (GDC) is an attractive electrolyte candidate for intermediate temperature SOFCs [74].

The anode should be capable of catalyzing fuel reforming when using hydrocarbon fuels [66]. Thus, porous electrodes (20%–40% porosity) are generally used to ensure gas diffusion. The chemical stability imposes requirements that electrodes do not react with the electrolytes or interconnects at operating temperatures. Preparation of ceramic composites, e.g., YSZ and GDC with metallic elements (Ni, Fe, Cu, etc.), is a feasible strategy for anode development. For example, nickel-doped YSZ has high ionic conductivity and catalytic activity and is highly chemically compatible as an anode for SOFCs with a YSZ electrolyte [64]. However, coke deposition because of the use of carbon fuels greatly deteriorates the catalytic activity of anode [75]; therefore, nickel-free anodes, such as $Sr_{1-x}La_xTiO_3$, are also an option to overcome this issue [76].

Perovskite-based materials like strontium-doped lanthanum manganite (LSM) are popular cathode materials for SOFCs because of their high electronic conductivity (~100 $S \cdot cm^{-1}$ for LSM at 600°C) and the proper thermal expansion coefficient matching that of the YSZ electrolyte [66]. Furthermore, penetration of the electrolyte components into the cathode structure may significantly decrease the contact resistance and mitigate the mismatch between the electrode and electrolyte, hence improving the cell performance [77].

4.5.2. SOFC performance and challenges

There are still many challenges of the SOFC technology and successful commercialization. The current material cost of electrolytes and electrodes (containing rare earth or other scarce elements) makes SOFC less competitive for large-scale applications. Furthermore, the high temperature is not favorable for viable commercialization, for increasing system costs and performance degradation. A lower operating temperature (<650°C) is expected to reduce the system cost and expand the choice for interconnects, insulations, and seal materials, as well as decrease the performance degradation rate [78]. However, reducing the temperature is always accompanied by reducing the catalyst activity and hence the fuel cell performance. Many efforts have been made to find low-cost electrolyte and electrode materials with high ionic conductivity and catalytic activity at reduced temperatures. Samarium and gadolinium doped ceria (SDC and GDC, respectively), as well as erbia-stabilized bismuth oxide, are promising electrolyte candidates for low-temperature operation because they have desirable ionic conductivity at reduced temperatures (0.1 $S \cdot cm^{-1}$ at 800°C for SDC, comparable to that of YSZ at 1000°C) [78]. In addition, ceria–salt composites ($LiNaCO_3$–SDC) may also overcome the problematic electronic conductivity of SDC [76]. In addition to the material selection, the decreasing area-specific reaction rate at reduced temperatures can be compensated by reducing the particle size of catalysts from microscale to nanoscale so that a triple-phase boundary density increases proportionally to reduce activation polarization [78]. Once the operating temperature is decreased, metal-supported SOFCs will be considered the next generation technology because of high mechanical strength, low cost, and excellent electrical conduction.

5. Conclusions and perspectives

Hydrogen as a clean and effective energy carrier has drawn great interest for a future carbon-neutral society based on renewable energies. The viability of the hydrogen chain in the framework of renewable energies has been well proven. The central linking technologies are water electrolysis, hydrogen storage, and fuel cells, which are briefly reviewed with the emphasis on their status and challenges.

Water electrolysis is a well-recognized technology in nearly all visions of future energy systems based on renewable sources. Alkaline electrolyzers are a mature technology on an industrial scale of MW; however, their dynamic performance needs to be improved to match the intermittent generation of renewable powers. Proton exchange membrane electrolyzers are compact in design and fast in the load response; however, the scarcity of precious metal-based catalysts and the high cost of corrosion-resistant construction materials are limitations to large-scale applications. Solid oxide electrolyte electrolyzers are under active development.

Effective storage and transport of hydrogen as the energy carrier are essential for the entire technological chain. Com-

pressed hydrogen gas at pressures up to 70 MPa is an established option for automobile applications. Alternative modes that are under development include metal hydrides and organic liquids. Alternatively, hydrogen can be carried as synthetic fuels, such as low carbon alcohols; however, the release of hydrogen while carrying chemicals is often energy intensive.

Fuel cells are an electrochemical energy conversion device that most favorably fits hydrogen because the electrochemical oxidation and reduction of hydrogen are highly reversible. Various types of fuel cells meet the diverse demands of hydrogen energy conversion. PEMFCs and SOFCs are the dominating technologies in automobile and stationary applications, respectively. Commercialization of fuel cells, particularly for automobiles, is more restrained by the unavailability of the hydrogen fueling infrastructure, while other issues include the long-term durability with start–stop cycling and the cost-effectiveness of the technology in comparison with the analog internal combustion engines.

Acknowledgements

This work was supported by the National Natural Science Foundation of China (No. 51704017) and the International Communication Program for Young Scientists in USTB (No. QNXM20210010). Xuan Liu also acknowledges the financial support from the China Scholarship Council, which enabled his research visit to Technical University of Denmark in 2021.

Conflict of Interest

All authors have no conflicts of interest.

References

[1] Intergovermental Panel on Climate Change (IPCC), *Sixth Assessment Report*, IPCC, Geneva, 2021 [2021-12-03]. https://www.ipcc.ch/assessment-report/ar6/

[2] T. Lockwood, A compararitive review of next-generation carbon capture technologies for coal-fired power plant, *Energy Procedia*, 114(2017), p. 2658.

[3] P. Millet and S. Grigoriev, Water electrolysis technologies, [in] L.M. Gandía, G. Arzamendi, and P.M. Diéguez, eds., *Renewable Hydrogen Technologies: Production, Purification, Storage, Applications and Safety*, Elsevier, Amsterdam, 2013, p. 19.

[4] J.J. Song, C. Wei, Z.F. Huang, C.T. Liu, L. Zeng, X. Wang, and Z.J. Xu, A review on fundamentals for designing oxygen evolution electrocatalysts, *Chem. Soc. Rev.*, 49(2020), No. 7, p. 2196.

[5] M. Carmo, D.L. Fritz, J. Mergel, and D. Stolten, A comprehensive review on PEM water electrolysis, *Int. J. Hydrogen Energy*, 38(2013), No. 12, p. 4901.

[6] I. Vincent and D. Bessarabov, Low cost hydrogen production by anion exchange membrane electrolysis: A review, *Renewable Sustainable Energy Rev.*, 81(2018), p. 1690.

[7] Q. Feng, X.Z. Yuan, G.Y. Liu, B. Wei, Z. Zhang, H. Li, and H.J. Wang, A review of proton exchange membrane water electrolysis on degradation mechanisms and mitigation strategies, *J. Power Sources*, 366(2017), p. 33.

[8] L. Bertuccioli, A. Chan, D. Hart, F. Lehner, B. Madden, and E. Standen, *Study on Development of Water Electrolysis in the EU*, Fuel Cells and Hydrogen Joint Undertaking, 2014 [2021-05-10]. https://www.fch.europa.eu/sites/default/files/FCHJUElectrolysisStudy_FullReport%20(ID%20199214).pdf

[9] C.C. Yang, S.F. Zai, Y.T. Zhou, L. Du, and Q. Jiang, Fe_3C-co nanoparticles encapsulated in a hierarchical structure of N-doped carbon as a multifunctional electrocatalyst for ORR, OER, and HER, *Adv. Funct. Mater.*, 29(2019), No. 27, art. No. 1901949.

[10] X.X. Zou and Y. Zhang, Noble metal-free hydrogen evolution catalysts for water splitting, *Chem. Soc. Rev.*, 44(2015), No. 15, p. 5148.

[11] L.H. Liu, N. Li, J.R. Han, K.L. Yao, and H.Y. Liang, Multicomponent transition metal phosphide for oxygen evolution, *Int. J. Miner. Metall. Mater.*, 29(2022), No. 3, p. 503.

[12] M. Lehner, R. Tichler, H. Steinmüller, and M. Koppe, *Power-to-Gas: Technology and Business Models*, Springer, New York, 2014.

[13] B. Decourt, B. Lajoie, R. Debarre, and O. Soupa, *Hydrogen-based Energy Conversion. More than Storage: System Flexibility*, SBC Energy Institute, Paris, 2014.

[14] M.Y. Wang, Z. Wang, X.Z. Gong, and Z.C. Guo, The intensification technologies to water electrolysis for hydrogen production – A review, *Renewable Sustainable Energy Rev.*, 29(2014), p. 573.

[15] M.R. Kraglund, D. Aili, K. Jankova, E. Christensen, Q.F. Li, and J.O. Jensen, Zero-gap alkaline water electrolysis using ion-solvating polymer electrolyte membranes at reduced KOH concentrations, *J. Electrochem. Soc.*, 163(2016), No. 11, p. F3125.

[16] W.E. Mustain and P.A. Kohl, Improving alkaline ionomers, *Nat. Energy*, 5(2020), No. 5, p. 359.

[17] C.Q. Li and J.B. Baek, The promise of hydrogen production from alkaline anion exchange membrane electrolyzers, *Nano Energy*, 87(2021), art. No. 106162.

[18] U. Babic, M. Suermann, F.N. Büchi, L. Gubler, and T.J. Schmidt, Critical review—Identifying critical gaps for polymer electrolyte water electrolysis development, *J. Electrochem. Soc.*, 164(2017), No. 4, p. F387.

[19] L.G. Li, P.T. Wang, Q. Shao, and X.Q. Huang, Metallic nanostructures with low dimensionality for electrochemical water splitting, *Chem. Soc. Rev.*, 49(2020), No. 10, p. 3072.

[20] N.T. Suen, S.F. Hung, Q. Quan, N. Zhang, Y.J. Xu, and H.M. Chen, Electrocatalysis for the oxygen evolution reaction: Recent development and future perspectives, *Chem. Soc. Rev.*, 46(2017), No. 2, p. 337.

[21] A. Hauch, S.D. Ebbesen, S.H. Jensen, and M. Mogensen, Highly efficient high temperature electrolysis, *J. Mater. Chem.*, 18(2008), No. 20, art. No. 2331.

[22] M.A. Laguna-Bercero, Recent advances in high temperature electrolysis using solid oxide fuel cells: A review, *J. Power Sources*, 203(2012), p. 4.

[23] K.F. Chen and S.P. Jiang, Review—Materials degradation of solid oxide electrolysis cells, *J. Electrochem. Soc.*, 163(2016), No. 11, p. F3070.

[24] P. Moçoteguy and A. Brisse, A review and comprehensive analysis of degradation mechanisms of solid oxide electrolysis cells, *Int. J. Hydrogen Energy*, 38(2013), No. 36, p. 15887.

[25] A. Ursua, L.M. Gandia, and P. Sanchis, Hydrogen production from water electrolysis: Current status and future trends, *Proc. IEEE*, 100(2012), No. 2, p. 410.

[26] N.T. Stetson, S. McWhorter, and C.C. Ahn, Introduction to hydrogen storage, [in] R.B. Gupta, A. Basile, and T.N. Veziroğlu, eds., *Compendium of Hydrogen Energy. Volume 2: Hydrogen Storage, Distribution and Infrastructure*, Woodhead Publishing, Cambrige, 2016, p. 3.

[27] E.W. Lemmon, M.O. McLinden, and D.G. Friend, Thermophysical properties of fluid systems, [in] P.J. Linstrom and

W.G. Mallard, eds., *NIST Chemistry Webbook, NIST Standard Reference Database*, Vol. 69, National Institute of Standards and Technology, Gaithersburg, MD, 1998.

[28] N. Stetson and M. Wieliczko, Hydrogen technologies for energy storage: A perspective, *MRS Energy Sustainability*, 7(2020), No. 1, art. No. 41.

[29] S. McWhorter and G. Ordaz, *Onboard Type IV Compressed Hydrogen Storage Systems – Current Performance and Cost*, DOE Fuel Cell Technologies Office, 2013 [2021-10-24]. https://www.hydrogen.energy.gov/pdfs/13010_onboard_storage_performance_cost.pdf

[30] NPROXX, *Stationary Hydrogen Storage Applications* [2021-11-10]. https://www.nproxx.com/hydrogen-storage-transport/stationary-applications/

[31] Hexagon, *Hydrogen Storage and Distribution – Lightweight High-Pressure Systems for Hydrogen Storage & Distribution* [2021-06-05]. https://hexagongroup.com/solutions/storage-distribution/hydrogen/

[32] Composite Advanced Technologies, LLC, *Highway to Hydrogen* [2021-12-01]. https://www.catecgases.com/hydrogen

[33] NPROXX, *Hydrogen Storage for Filling Stations* [2021-11-13]. https://www.nproxx.com/hydrogen-storage-transport/hydrogen-refuelling-stations/

[34] K.L. Simmons, *Synergistically Enhanced Materials and Design Parameters for Reducing the Cost of Hydrogen Storage Tanks*, DOE Hydrogen and Fuel Cells Program, 2014 [2021-10-20]. https://www.hydrogen.energy.gov/pdfs/progress14/iv_f_3_simmons_2014.pdf

[35] A.S. Lord, P.H. Kobos, and D.J. Borns, Geologic storage of hydrogen: Scaling up to meet city transportation demands, *Int. J. Hydrogen Energy*, 39(2014), No. 28, p. 15570.

[36] J. Michalski, U. Bünger, F. Crotogino, S. Donadei, G.S. Schneider, T. Pregger, K.K. Cao, and D. Heide, Hydrogen generation by electrolysis and storage in salt caverns: Potentials, economics and systems aspects with regard to the German energy transition, *Int. J. Hydrogen Energy*, 42(2017), No. 19, p. 13427.

[37] R. K. Ahluwalia, J.K. Peng, H.S. Roh, and D. Papadias, *System Analysis of Physical and Materials-Based Hydrogen Storage*, DOE Hydrogen and Fuel Cells Program, 2019 [2021-09-10]. https://www.hydrogen.energy.gov/pdfs/progress19/h2f_st001_ahluwalia_2019.pdf

[38] R.R. Ratnakar, N. Gupta, K. Zhang, C. van Doorne, J. Fesmire, B. Dindoruk, and V. Balakotaiah, Hydrogen supply chain and challenges in large-scale LH2 storage and transportation, *Int. J. Hydrogen Energy*, 46(2021), No. 47, p. 24149.

[39] V. Tietze, S. Luhr, and D. Stolten, Bulk storage vessels for compressed and liquid hydrogen, [in] D. Stolten and B. Emonts, eds., *Hydrogen Science and Engineering: Materials, Processes, Systems and Technology*, Wiley-VCH, Weinheim, 2016, p. 659.

[40] J. Andersson and S. Grönkvist, Large-scale storage of hydrogen, *Int. J. Hydrogen Energy*, 44(2019), No. 23, p. 11901.

[41] G. Valenti, Hydrogen liquefaction and liquid hydrogen storage, [in] *Compendium of Hydrogen Energy. Volume 2: Hydrogen Storage, Distribution and Infrastructure*, Woodhead Publishing, Cambridge, 2016, p. 27.

[42] A. Züttel, Hydrogen storage methods, *Naturwissenschaften*, 91(2004), No. 4, p. 157.

[43] J.B. von Colbe, J.R. Ares, J. Barale, M. Baricco, C. Buckley, G. Capurso, N. Gallandat, D.M. Grant, M.N. Guzik, I. Jacob, E.H. Jensen, T. Jensen, J. Jepsen, T. Klassen, M.V. Lototskyy, K. Manickam, A. Montone, J. Puszkiel, S. Sartori, D.A. Sheppard, A. Stuart, G. Walker, C.J. Webb, H. Yang, V. Yartys, A. Züttel, and M. Dornheim, Application of hydrides in hydrogen storage and compression: Achievements, outlook and perspectives, *Int. J. Hydrogen Energy*, 44(2019), No. 15, p. 7780.

[44] C. Milanese, T.R. Jensen, B.C. Hauback, C. Pistidda, M. Dornheim, H. Yang, L. Lombardo, A. Zuettel, Y. Filinchuk, P. Ngene, P.E. de Jongh, C.E. Buckley, E.M. Dematteis, and M. Baricco, Complex hydrides for energy storage, *Int. J. Hydrogen Energy*, 44(2019), No. 15, p. 7860.

[45] M. Hirscher, V.A. Yartys, M. Baricco, J.B. von Colbe, D. Blanchard, R.C. Bowman, D.P. Broom, C.E. Buckley, F. Chang, P. Chen, Y.W. Cho, J.C. Crivello, F. Cuevas, W.I.F. David, P.E. de Jongh, R.V. Denys, M. Dornheim, M. Felderhoff, Y. Filinchuk, G.E. Froudakis, D.M. Grant, E.M. Gray, B.C. Hauback, T. He, T.D. Humphries, T.R. Jensen, S. Kim, Y. Kojima, M. Latroche, H.W. Li, M.V. Lototskyy, J.W. Makepeace, K.T. Møller, L. Naheed, P. Ngene, D. Noréus, M.M. Nygård, S.I. Orimo, M. Paskevicius, L. Pasquini, D.B. Ravnsbæk, M.V. Sofianos, T.J. Udovic, T. Vegge, G.S. Walker, C.J. Webb, C. Weidenthaler, and C. Zlotea, Materials for hydrogen-based energy storage – Past, recent progress and future outlook, *J. Alloys Compd.*, 827(2020), art. No. 153548.

[46] Q. Li, X. Lin, Q. Luo, Y.A. Chen, J.F. Wang, B. Jiang, and F.S. Pan, Kinetics of the hydrogen absorption and desorption processes of hydrogen storage alloys: A review, *Int. J. Miner. Metall. Mater.*, 29(2022), No. 1, p. 32.

[47] T. He, P. Pachfule, H. Wu, Q. Xu, and P. Chen, Hydrogen carriers, *Nat. Rev. Mater.*, 1(2016), No. 12, art. No. 16059.

[48] A. Bourane, M. Elanany, T.V. Pham, and S.P. Katikaneni, An overview of organic liquid phase hydrogen carriers, *Int. J. Hydrogen Energy*, 41(2016), No. 48, p. 23075.

[49] S. Bradley and W. Wilczewski, Power-to-gas brings a new focus to the issue of energy storage from renewable sources, *Today in Energy*, 2015 [2021-11-21]. https://www.eia.gov/todayinenergy/detail.php?id=22212#

[50] FIBA Technologies, *Superjumbo Tube Trailers*, FIBA Technologies, Inc, Littleton [2021-12-09]. https://www.fibatech.com/products/tube-trailers-and-skids/superjumbo-tube-trailers/

[51] P. Schnell, Refueling station layout, [in] D. Stolten and B. Emonts, eds., *Hydrogen Science and Engineering: Materials, Processes, Systems and Technology*, Wiley-VCH, Weinheim, 2016, p. 891.

[52] R. Gerboni, Introduction to hydrogen transportation, [in] R.B. Gupta, A. Basile, and T.N. Veziroğlu, eds., *Compendium of Hydrogen Energy. Volume 2: Hydrogen Storage, Distribution and Infrastructure*, Woodhead Publishing, Cambrige, 2016, p. 283.

[53] R.C. Samsun, L. Antoni, M. Rex, and D. Stolten, *Deployment Status of Fuel Cells in Road Transport: 2021 Update*, Forschungszentrum Jülich GmbH, Zentralbibliothek, Verlag, Jülich, 2021.

[54] D. Apostolou and G. Xydis, A literature review on hydrogen refuelling stations and infrastructure. Current status and future prospects, *Renewable Sustainable Energy Rev.*, 113(2019), art. No. 109292.

[55] S. Chubbock and R. Clague, Comparative analysis of internal combustion engine and fuel cell range extender, *SAE Int. J. Alt. Power.*, 5(2016), No. 1, p. 175.

[56] A. Elgowainy and M.Q. Wang, *Fuel Cycle Comparison of Distributed Power Generation Technologies*, Office of Scientific and Technical Information (OSTI), Oak Ridge, TN, 2008 [2021-11-02]. https://www.osti.gov/biblio/946042-qtnABP/

[57] Y.J. Wang, J.L. Qiao, R. Baker, and J.J. Zhang, Alkaline polymer electrolyte membranes for fuel cell applications, *Chem. Soc. Rev.*, 42(2013), No. 13, p. 5768.

[58] J.R. Varcoe, P. Atanassov, D.R. Dekel, A.M. Herring, M.A. Hickner, P.A. Kohl, A.R. Kucernak, W.E. Mustain, K. Nijmeijer, K. Scott, T.W. Xu, and L. Zhuang, Anion-exchange membranes in electrochemical energy systems, *Energy Environ. Sci.*, 7(2014), No. 10, p. 3135.

[59] Q.F. Li, D. Aili, H.A. Hjuler, and J.O. Jensen, *High Temperature Polymer Electrolyte Membrane Fuel Cells: Approaches, Status, and Perspectives*, Springer, Cham, 2016.

[60] L.X. Fan, Z.K. Tu, and S.H. Chan, Recent development of hydrogen and fuel cell technologies: A review, *Energy Rep.*, 7(2021), p. 8421.
[61] M. Cassir, A. Meléndez-Ceballos, A. Ringuedé, and V. Lair, Molten carbonate fuel cells, [in] F. Barbir, A. Basile, and T.N. Veziroğlu, eds., *Compendium of Hydrogen Energy. Volume 3: Hydrogen Energy Conversion*, Woodhead Publishing, Cambridge, 2016, p. 71.
[62] A.S. Mehr, A. Lanzini, M. Santarelli, and M.A. Rosen, Polygeneration systems based on high temperature fuel cell (MCFC and SOFC) technology: System design, fuel types, modeling and analysis approaches, *Energy*, 228(2021), art. No. 120613.
[63] M. Singh, D. Zappa, and E. Comini, Solid oxide fuel cell: Decade of progress, future perspectives and challenges, *Int. J. Hydrogen Energy*, 46(2021), No. 54, p. 27643.
[64] B.S. Prakash, S.S. Kumar, and S.T. Aruna, Properties and development of Ni/YSZ as an anode material in solid oxide fuel cell: A review, *Renewable Sustainable Energy Rev.*, 36(2014), p. 149.
[65] Z. Zakaria, Z. Awang Mat, S.H. Abu Hassan, and Y. Boon Kar, A review of solid oxide fuel cell component fabrication methods toward lowering temperature, *Int. J. Energy Res.*, 44(2020), No. 2, p. 594.
[66] N. Mahato, A. Banerjee, A. Gupta, S. Omar, and K. Balani, Progress in material selection for solid oxide fuel cell technology: A review, *Prog. Mater. Sci.*, 72(2015), p. 141.
[67] R.K. Mallick, S.B. Thombre, and N.K. Shrivastava, Vapor feed direct methanol fuel cells (DMFCs): A review, *Renewable Sustainable Energy Rev.*, 56(2016), p. 51.
[68] B.G. Pollet, A.A. Franco, H. Su, H. Liang, and S. Pasupathi, Proton exchange membrane fuel cells, [in] F. Barbir, A. Basile, and T.N. Veziroğlu, eds., *Compendium of Hydrogen Energy. Volume 3: Hydrogen Energy Conversion*, Woodhead Publishing, Cambridge, 2016, p. 3.
[69] L.Y. Zhu, Y.C. Li, J. Liu, J. He, L.Y. Wang, and J.D. Lei, Recent developments in high-performance Nafion membranes for hydrogen fuel cells applications, *Pet. Sci.*, (2021). https://doi.org/10.1016/j.petsci.2021.11.004
[70] D. Van Dao, G. Adilbish, I.H. Lee, and Y.T. Yu, Enhanced electrocatalytic property of Pt/C electrode with double catalyst layers for PEMFC, *Int. J. Hydrogen Energy*, 44(2019), No. 45, p. 24580.
[71] E. Middelman, Improved PEM fuel cell electrodes by controlled self-assembly, *Fuel Cells Bull.*, 2002(2002), No. 11, p. 9.
[72] J.F. Lin, J. Wertz, R. Ahmad, M. Thommes, and A.M. Kannan, Effect of carbon paper substrate of the gas diffusion layer on the performance of proton exchange membrane fuel cell, *Electrochim. Acta*, 55(2010), No. 8, p. 2746.
[73] K. Panagi, C.J. Laycock, J.P. Reed, and A.J. Guwy, Highly efficient coproduction of electrical power and synthesis gas from biohythane using solid oxide fuel cell technology, *Appl. Energy*, 255(2019), art. No. 113854.
[74] M. Choolaei, Q. Cai, R.C.T. Slade, and B. Amini Horri, Nanocrystalline gadolinium-doped ceria (GDC) for SOFCs by an environmentally-friendly single step method, *Ceram. Int.*, 44(2018), No. 11, p. 13286.
[75] M.Z. Ahmad, S.H. Ahmad, R.S. Chen, A.F. Ismail, R. Hazan, and N.A. Baharuddin, Review on recent advancement in cathode material for lower and intermediate temperature solid oxide fuel cells application, *Int. J. Hydrogen Energy*, 47(2022), No. 2, p. 1103.
[76] C. Xia, Y. Li, Y. Tian, Q.H. Liu, Z.M. Wang, L.J. Jia, Y.C. Zhao, and Y.D. Li, Intermediate temperature fuel cell with a doped ceria–carbonate composite electrolyte, *J. Power Sources*, 195(2010), No. 10, p. 3149.
[77] A. Ahuja, M. Gautam, A. Sinha, J. Sharma, P.K. Patro, and A. Venkatasubramanian, Effect of processing route on the properties of LSCF-based composite cathode for IT-SOFC, *Bull. Mater. Sci.*, 43(2020), No. 1, art. No. 129.
[78] E.D. Wachsman and K.T. Lee, Lowering the temperature of solid oxide fuel cells, *Science*, 334(2011), No. 6058, p. 935.